Journal of Biomolecular NMR, 8 (1996) 379–390
ESCOM



J-Bio NMR 403

# Solution structure of human neuropeptide Y

Stephen A. Monks[a], Gloria Karagianis[a], Geoffrey J. Howlett[b] and Raymond S. Norton[a,*]

[a]*Biomolecular Research Institute, 343 Royal Parade, Parkville 3052, VIC, Australia*
[b]*Department of Biochemistry and Molecular Biology, University of Melbourne, Parkville 3052, VIC, Australia*

Received 17 June 1996
Accepted 16 August 1996

*Keywords:* Structure; Helix; Polypeptide; Self-association

**Summary**

The three-dimensional structure of synthetic human neuropeptide Y in aqueous solution at pH 3.2 and 37 °C was determined from two-dimensional $^1$H NMR data recorded at 600 MHz. A restraint set consisting of 440 interproton distance restraints inferred from NOEs and 11 backbone and 4 side-chain dihedral angle restraints derived from spin–spin coupling constants was used as input for distance geometry calculations in DIANA and simulated annealing and restrained energy minimisation in X-PLOR. The final set of 26 structures is well defined in the region of residues 11 36, with a mean pairwise rmsd of 0.51 Å for the backbone heavy atoms (N, $C^\alpha$ and C) and 1.34 Å for all heavy atoms. Residues 13–36 form an amphipathic α-helix. The N-terminal 10 residues are poorly defined relative to the helical region, although some elements of local structure are apparent. At least one of the three prolines in this N-terminal region co-exists in both cis and trans conformations. An additional set of 24 distances was interpreted as intermolecular distances within a dimer. A combination of distance geometry and restrained simulated annealing yielded a model of the dimer having antiparallel packing of two helical units, whose hydrophobic faces form a well-defined core. Sedimentation equilibrium experiments confirm the observation that neuropeptide Y associates to form dimers and higher aggregates under the conditions of the NMR experiments. Our results therefore support the structural features reported for porcine neuropeptide Y [Cowley, D.J. et al. (1992) *Eur. J. Biochem.*, **205**, 1099–1106] rather than the 'aPP' fold described previously for human neuropeptide Y [Darbon, H. et al. (1992) *Eur. J. Biochem.*, **209**, 765–771].

## Introduction

Neuropeptide Y (NPY) is a 36-residue, C-terminally amidated polypeptide hormone and neurotransmitter, acting in both the central and peripheral nervous systems. It is the most abundant mammalian neuropeptide identified to date and is believed to be involved in the regulation of several physiological parameters, notably food intake, blood pressure, circadian rhythms and sexual behaviour (Colmers and Wahlestedt, 1993; Grundemar and Håkanson, 1994). Three receptor subtypes ($Y_1$, $Y_2$ and $Y_3$) have been identified for NPY (Gray and Morley, 1986; Grundemar et al., 1993), but the structural basis for its biological activity remains poorly understood.

NPY is a member of the pancreatic polypeptide (PP) family and has ca. 50% sequence identity with avian PP, for which a crystal structure exists (Blundell et al., 1981). Avian PP forms a symmetrical dimer in the crystal state, with each monomer consisting of an N-terminal polyproline-like helix (residues 1–8) and a C-terminal α-helix (residues 14–31), closely associated to form a hairpin fold. This fold is stabilised by hydrophobic interactions between the N- and C-terminal nonpolar residues, and the dimer is stabilised principally by the interlocking of nonpolar groups from the α-helices. The nonhelical C-terminus (residues 32–36) is rather flexible and extends away from the bulk of the molecule.

The structure of human NPY in aqueous solution has

*To whom correspondence should be addressed.

*Abbreviations:* NPY, neuropeptide Y; PP, pancreatic polypeptide; 1D, 2D, one-, two-dimensional; NOE, nuclear Overhauser enhancement; NOESY, 2D NOE spectroscopy; TOCSY, 2D total correlation spectroscopy; E.COSY, exclusive correlation spectroscopy; HMQC, heteronuclear multiple-quantum coherence; rmsd, root-mean-square deviation.

been investigated recently by 2D $^1$H NMR (Darbon et al., 1992) and was reported to have an 'aPP'-like fold, with no evidence of self-association. In this monomeric model, two short contiguous α-helices encompassing residues 15–26 and 28–35 are linked by a hinge, forming an angle of 100°. By contrast, in the NMR-based structure of porcine NPY in aqueous solution at 37 °C, the C-terminal segment (residues 11–36) formed an amphipathic α-helix while the N-terminus remained unstructured, and dimers involving intermolecular helix–helix interactions were present in solution (Cowley et al., 1992). Different structures for NPY have been obtained from 2D $^1$H NMR data acquired in other solvents. In 2,2,2-trifluoroethanol-$d_3$:water (9:1) at low pH and at 35 °C, residues 19–34 of human NPY formed an α-helix, the N-terminus was disordered and no dimer formation was evident (Mierke et al., 1992). By contrast, an analogue of residues 13-36 of human NPY in 20% (v/v) trifluoroethanol-$d_3$ in water did form a dimer (Barden, 1995). In DMSO-$d_6$ at 30 °C, human NPY had no α-helical secondary structure but two β-turns were present which allowed the molecule to adopt a hairpin fold, bringing the N- and C-termini into close proximity (Boulanger et al., 1995).

Using solution conditions similar to those of Darbon et al. (1992), we have found human NPY to undergo self-association at least to the level of dimers and we have not observed long-range intramolecular NOEs consistent with an 'aPP'-like fold for the monomer. Rather, our data suggest that the NPY molecules associate via interactions of the hydrophobic residues in the α-helical region encompassing residues 13–36. This observation is more consistent with the solution structure of porcine NPY, which is an intertwined dimer (Cowley et al., 1992). We present a three-dimensional model of the NPY dimer, generated from the set of intra- and intermolecular NOE distance constraints derived from our NMR data and used as input into a combination of distance geometry, simulated annealing and molecular dynamics calculations.

## Materials and Methods

*Sample preparation*

Synthetic human NPY and porcine NPY were obtained from Auspep Pty. Ltd. (Melbourne, Australia; > 98% purity according to analytical reversed-phase HPLC in water/acetonitrile containing 0.1% trifluoroacetic acid). The molecular mass of human NPY was determined to be 4273.0 Da by laser desorption mass spectrometry, in excellent agreement with the theoretical mass of 4272.0 Da. NMR samples were prepared by dissolving the peptide in either 90% (v/v) $H_2O$/10% (v/v) $D_2O$ or 99.96% $D_2O$. The pH was adjusted by adding small amounts of 0.1 M NaOD or DCl. Reported pH values were measured at room temperature and are uncorrected for deuterium isotope effects. Sample concentrations were in the range 4–5 mM, unless otherwise stated. $D_2O$ (99.96% deuterated) was obtained from Cambridge Isotope Laboratories (Woburn, MA, U.S.A.).

*Analytical ultracentrifugation*

Sedimentation equilibrium experiments were performed using the Beckman XLA ultracentrifuge and Ti60 rotor. A 12 mm centrepiece and a sample volume of 100 µl were used in experiments with low starting concentrations of human NPY, whereas at high starting concentrations a 4 mm path length centrepiece and a sample volume of 45 µl were used. Sedimentation equilibrium distributions were formed by centrifugation at 40 000 rpm for 18 h at 20 °C and the absorbance profiles were measured using wavelengths from 230 to 290 nm, as indicated. Data were analysed initially by nonlinear regression assuming a single species, and a value of 0.714 mg/ml for the partial specific volume of the peptide was calculated from the amino acid composition. Models for self-association of the peptide were examined by global analysis of the data obtained at different starting concentrations using the program MULTEQ, kindly provided by Dr. A.P. Minton (NIH, Bethesda, MD, U.S.A.).

*NMR spectroscopy*

$^1$H NMR spectra were recorded on Bruker AMX-500 and AMX-600 spectrometers, with the probe temperature maintained at 37 °C using a B-VT1000E control unit connected to a Haake cooling bath. In all experiments, the carrier was set in the centre of the spectrum and quadrature detection was used in both dimensions. All 2D spectra were recorded in the phase-sensitive mode using the time-proportional phase incrementation method (Marion and Wüthrich, 1983). NOESY spectra (Anil Kumar et al., 1980; Macura et al., 1981) were recorded with mixing times of 65, 125, 200 and 300 ms. TOCSY spectra (Braunschweiler and Ernst, 1983) were recorded using the DIPSI-2 spin-lock sequence (Rucker and Shaka, 1989) and spin-lock times of 12.4 or 60–70 ms. An E.COSY experiment (Griesinger et al., 1987) was recorded in 99.96% $D_2O$ to measure $^3J_{C^\alpha H C^\beta H}$ coupling constants and a $^{13}$C-HMQC experiment (Bax et al., 1983) was recorded in $D_2O$ to obtain $^{13}$C chemical shifts.

Solvent suppression was carried out using selective, low-power irradiation of the water resonance during the relaxation delay (1.8 s) and, in the case of NOESY experiments, also during the mixing time. The spectral width was 6098.0 Hz, acquired over 4096 data points. Typically, 450 $t_1$ increments were acquired, with 40 to 96 scans per increment. For the E.COSY experiment, 900 $t_1$ increments of 48 scans with 4096 data points in $t_2$ were collected in order to achieve the required high digital resolution. The $^{13}$C-HMQC was recorded at 500 MHz using $^1$H and $^{13}$C sweep widths of 5555.6 and 10 061.1 Hz,

respectively, with 512 $t_1$ increments and 208 scans per increment acquired over 4096 data points.

Data were processed on a Bruker X32 workstation, using the manufacturer's program UXNMR. Before Fourier transformation and baseline correction, sine-squared window functions, with phase shifts of 45° to 90°, were applied in both dimensions. Final matrix sizes were usually 2048 × 2048 real points (4096 real points were used in $t_2$ for the E.COSY spectrum). Data analysis was carried out using the software package FELIX (v. 2.05 and 2.1, Biosym Technologies, San Diego, CA, U.S.A.) running on Silicon Graphics IRIS 4D/30 workstations.

In the course of our NMR studies of human NPY, extra $C^{\alpha}H$-NH cross peaks were observed in a 2D TOSCY experiment acquired approximately 5 months after the preparation of one sample (which was stored at 4 °C between recording of spectra), suggesting that degradation had occurred. Degradation was confirmed by reversed-phase HPLC, which showed two major peaks, and by mass spectrometry, which indicated, in order of increasing relative intensity, cleavage at the amide bonds between residues $Pro^8$-$Gly^9$, $Asp^6$-$Asn^7$ and $Asp^{11}$-$Ala^{12}$. A fresh sample was prepared for the measurement of structural restraints.

*Structure determination*

Structural restraints were derived primarily from NOESY spectra recorded with a mixing time of 200 ms. A small number of constraints was also derived from 200 ms NOESY spectra recorded at pH 2.9 and 3.6 in $H_2O$ and at pH 3.2 in $D_2O$. NOESY spectra were processed using a 90°-shifted sine-bell function in both dimensions. Cross-peak volumes were integrated using FELIX and those cross peaks representing degenerate protons were divided by the appropriate factor before conversion to distances. Peak volumes were calibrated using an average value of the volumes from four well-resolved geminal $C^{\beta}H$ cross peaks ($Asn^7$, $Arg^{25}$, $His^{26}$ and $Tyr^{36}$) and the five well-resolved tyrosine aromatic protons. After conversion of the volumes to distances, corrections of 0.5 and 1.0 Å were added to distance restraints involving backbone protons only and at least one side-chain proton, respectively.

Dihedral angle constraints for residues $Ala^{12}$, $Ala^{14}$, $Glu^{15}$, $Tyr^{21}$, $Leu^{24}$ and $Arg^{25}$ were inferred from $^3J_{HNC^{\alpha}H}$ coupling constants derived directly from the 1D spectrum and for residues $Asp^{16}$, $Met^{17}$, $Ala^{18}$, $His^{26}$ and $Ile^{31}$ from peak amplitude evaluation of a short-mixing-time (12.4 ms) TOCSY experiment (Fogolari et al., 1993), with $\phi$ centred at $-60° \pm 40°$ for $^3J_{HNC^{\alpha}H} < 6$ Hz and at $-60° \pm 30°$ for $^3J_{HNC^{\alpha}H} < 5$ Hz. For residues whose coupling constant could be measured from the 1D spectrum, there was good agreement with values calculated using the short-mixing-time TOCSY. Backbone dihedral restraints were not applied for $^3J_{HNC^{\alpha}H}$ values between 6 and 8 Hz. Coupling constants could not be measured accurately from a DQF-COSY experiment, as the cross peaks were severely attenuated by line broadening. Nondegenerate $C^{\beta}H$ resonances were observed for 22 residues at pH 3.2 and 37 °C (see Results). Where possible, $^3J_{C^{\alpha}H C^{\beta}H}$ coupling constants were measured from the passive couplings displaced in the E.COSY spectrum and the relative intensities of the intraresidue $d_{\alpha\beta}$ NOEs measured from a 50 ms NOESY spectrum recorded under the same conditions. Four residues were found to have patterns consistent with one of the three possible staggered conformations for $\chi^1$ and were restrained as follows: $Asn^7$: $\chi^1 = 60° \pm 40°$; $Asp^{11}$: $\chi^1 = -60° \pm 40°$; $His^{26}$: $\chi^1 = 180° \pm 40°$ and $Tyr^{36}$: $\chi^1 = -60° \pm 40°$ (Hyberts et al., 1987; Wagner et al., 1987).

Pseudo-atom corrections were added for degenerate methylene, methyl and tyrosine ring protons, with values of 0.9, 1.1 and 2.4 Å, respectively. Restraints to nondegenerate methylene protons which were not stereospecifically assigned were corrected automatically by the DIANA program (Güntert et al., 1991). For calculations in X-PLOR (Brünger, 1992), the upper and lower bound distance restraints from DIANA were converted to X-PLOR format using an in-house program and restraints for the tyrosine ring protons were reinterpreted for separate (2,6) and (3,5) pseudo-atoms (correction of 2.2 Å).

Preliminary structures of the monomer were generated with the distance geometry program DIANA (v. 2.1), with the use of stereospecific assignments and dihedral

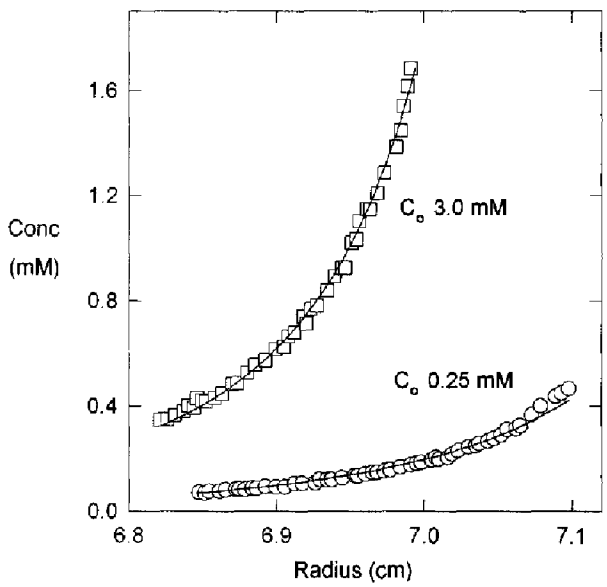


Fig. 1. Sedimentation equilibrium analysis of human NPY. Centrifugation was done at 40 000 rpm for 18 h at 20 °C. Solution conditions were 0.1 M NaCl, pH 3.1 and the initial concentrations of NPY were 0.25 mM (○) and 3 mM (□). Data were collected at a wavelength of 285 nm using an XLA analytical ultracentrifuge. The concentration (in mM) is plotted against the radial position. The solid lines describe the theoretical behaviour of a reversibly associating system governed by equilibrium constants of 697 $M^{-1}$ for the monomer–dimer interaction and 1040 $M^{-1}$ for the dimer–tetramer interaction.

angle constraints derived from coupling constant data and distance constraints ($|i-j| \leq 4$) derived from NOE cross peaks that had been assigned unambiguously in both chemical shift dimensions. No hydrogen bonding constraints were used in the calculations. The standard search protocol and parameters for DIANA were employed. Additional NOESY cross-peak assignments were then made based on interproton distances in these initial structures. Several rounds of structure calculations were carried out before the restraint list was finalised. In the final stages of the DIANA calculations, 54 lower bounds were increased to 3.5 Å as described by Pallaghy et al. (1995).

The 75 structures with the lowest DIANA penalty functions were submitted to a simulated annealing protocol in X-PLOR, v. 3.1. The all-hydrogen distance geometry force field was employed, which includes covalent geometry, planarity and hard-sphere van der Waals terms but no Lennard-Jones, electrostatic or empirical dihedral angle (apart from planarity) terms. The standard simulated annealing macro sa.inp was used, with a modification for prolines as described by Pallaghy et al. (1995). Simulated annealing was performed using 20 000 steps at 1000 K and 10 000 steps as the molecule was gradually cooled to 300 K. A time step of 1 fs was employed throughout. The initial van der Waals weighting was very low (0.002), so as to allow atoms to pass through each other early in the simulation.

Each structure was then submitted to a restrained simulated annealing refinement protocol, which makes 10 attempts to find a lower energy structure (Pallaghy et al., 1995). The macro cools the structures gradually from 300 to 0 K over 20 000 steps and is followed by 1000 steps of Powell conjugate gradient energy minimisation. The 50 structures with the lowest total and NOE energy were then selected and energy minimised in the empirical CHARMm force field (Brooks et al., 1983), with all explicit charges neutralized and using a distance-dependent dielectric. The force field was modified to leave the backbone $\phi$ and $\psi$ angles unconstrained by the empirical dihedral angle term; this was achieved by removing the relevant type-based dihedral terms from the parmallh3x.pro file. The 26 structures with the lowest total energy, excluding the Coulombic term contribution, constituted the final set used for structural analysis of the monomer. Hydrogen bonds were identified using INSIGHT (v. 2.3.0, Biosym Technologies, San Diego, CA, U.S.A.), which was also used for visualisation of structures and generation of diagrams, except as noted. The 26 structures and the NMR restraints used in their determination have been deposited with the Brookhaven Protein Data Bank (filename 1RON).

Starting structures for the dimer were generated by duplication of the monomer coordinates in a modified version of the procedure of Nilges (1993). The resulting dimer structures were submitted to a molecular dynamics–simulated annealing refinement protocol which involved three phases: (i) a conformational search phase at 2000 K; (ii) a cooling phase in which the system was cooled to 100 K; and (iii) a short conjugate gradient minimisation phase. The X-PLOR noncrystallographic symmetry term was used to maintain monomer symmetry, and the symmetry pseudo-NOE term was used to maintain symmetrical intermonomer contacts as described by Nilges (1993).

## Results

*Sedimentation equilibrium analysis*

The sedimentation equilibrium behaviour of human NPY, at pH 3.1 and 0.1 M NaCl concentration, was initially examined using a starting concentration of 0.021 mM and optical density measurements at 230 nm. Analysis of the data indicated a single sedimenting species with a molecular mass of $4100 \pm 50$ Da, in good agreement with the value calculated from the amino acid composition of the peptide (4272 Da). Sedimentation equilibrium distributions obtained at higher starting concentrations (0.25 and 3 mM) and monitored at 285 nm are presented in Fig. 1. Curve fitting of the data assuming a single species yielded apparent molecular masses of $5700 \pm 260$ and $6859 \pm 320$ Da, respectively. The magnitude of the values obtained, together with the relatively poor fits to the experimental data, indicated self-association. A global analysis of the sedimentation equilibrium data obtained at the higher starting concentrations allowed different models for the self-association to be tested. Curve fitting of the data assuming either a monomer–dimer equilibrium or a monomer–dimer–trimer equilibrium provided unsatisfactory fits. The simplest model to adequately describe the data was obtained for a monomer–dimer–tetramer system governed by equilibrium constants of 697 $M^{-1}$ for the monomer–dimer equilibrium and 1040 $M^{-1}$ for the dimer–tetramer equilibrium. These equilibrium constants were used to compute the theoretical lines shown in Fig. 1. At a concentration of 2.3 mM, this model predicts proportions of monomer, dimer and tetramer of 33, 36 and 31%, respectively.

Sedimentation equilibrium experiments with human NPY were also performed at pH 3.1 in the absence of added salt. Samples at initial concentrations of 0.023, 0.28 and 3.3 mM were centrifuged and equilibrium absorption profiles were collected at wavelengths of 230, 285 and 290 nm. Analysis of the data assuming a single species yielded estimates for the molecular mass of 2610, 1700 and 3000 Da, respectively. These values, which are low relative to the molecular mass of the monomeric NPY (4272 Da), are indicative of nonideality and significant charge effects (Schachman, 1959). The difficulty of assigning values to the ionic strength under these conditions prevented a more detailed analysis of the data in order to determine the nature of the molecular species present.

TABLE 1
PROTON CHEMICAL SHIFTS FOR HUMAN NPY[a]

| Residue | NH | $C^{\alpha}H$ | $C^{\beta}H$ | $C^{\gamma}H$ | Others |
|---|---|---|---|---|---|
| $Tyr^{1}$ | – | 4.48 | 3.24, 3.04 | | C(2,6)H 7.23; C(3,5)H 6.90 |
| $Pro^{2}$ | – | 4.54 | 2.27, 1.94 | 2.00 | $C^{\delta}H_2$ 3.71, 3.35 |
| $Ser^{3}$ | 8.34 | 4.46 | 3.88 | | |
| $Lys^{4}$ | 8.25 | 4.64 | 1.82, 1.70 | 1.45 | $C^{\delta}H_2$ 1.45; $C^{\epsilon}H_2$ 3.01; $N^{\zeta}H_3^{+}$ 7.50 |
| $Pro^{5}$ | – | 4.41 | 2.27, 1.91 | 1.99 | $C^{\delta}H_2$ 3.79, 3.62 |
| $Asp^{6}$ | 8.46 | 4.64 | 2.82, 2.77 | | |
| $Asn^{7}$ | 8.27 | 4.89 | 2.81, 2.66[b] | | $N^{\delta}H_2$ 7.54, 6.88 |
| $Pro^{8}$ | – | 4.41 | 2.26, 1.91 | 1.99 | $C^{\delta}H_2$ 3.71 |
| $Gly^{9}$ | 8.34 | 3.93 | | | |
| $Glu^{10}$ | 8.01 | 4.34 | 2.13, 2.00 | 2.44 | |
| $Asp^{11}$ | 8.36 | 4.71 | 2.88, 2.79[b] | | |
| $Ala^{12}$ | 8.04 | 4.55 | 1.37 | | |
| $Pro^{13}$ | – | 4.38 | 2.30, 1.90 | 2.05 | $C^{\delta}H_2$ 3.77, 3.66 |
| $Ala^{14}$ | 8.24 | 4.22 | 1.41 | | |
| $Glu^{15}$ | 8.27 | 4.25 | 2.08 | 2.45 | |
| $Asp^{16}$ | 8.20 | 4.51 | 2.81 | | |
| $Met^{17}$ | 8.14 | 4.33 | 2.08 | 2.64, 2.53 | $C^{\epsilon}H_3$ 2.00 |
| $Ala^{18}$ | 8.04 | 4.17 | 1.48 | | |
| $Arg^{19}$ | 7.86 | 4.12 | 1.81, 1.76 | 1.61, 1.50 | $C^{\delta}H_2$ 3.15; $N^{\epsilon}H$ 7.16; $N^{\eta}H_2$ 6.64 |
| $Tyr^{20}$ | 7.86 | 4.44 | 3.05, 3.01 | | C(2,6)H 6.91; C(3,5)H 6.72 |
| $Tyr^{21}$ | 8.28 | 4.26 | 3.09, 3.03 | | C(2,6)H 7.10; C(3,5)H 6.79 |
| $Ser^{22}$ | 8.15 | 4.17 | 4.00, 3.94 | | |
| $Ala^{23}$ | 7.94 | 4.20 | 1.37 | | |
| $Leu^{24}$ | 8.11 | 4.09 | 1.64 | 1.64 | $C^{\delta}H_3$ 0.87 |
| $Arg^{25}$ | 8.08 | 3.93 | 1.80, 1.65 | 1.48 | $C^{\delta}H_2$ 3.11; $N^{\epsilon}H$ 7.17; $N^{\eta}H_2$ 6.64 |
| $His^{26}$ | 8.03 | 4.42 | 3.29, 3.20[b] | | C(2)H 8.59; C(4)H 6.84 |
| $Tyr^{27}$ | 8.17 | 4.21 | 3.06, 2.99 | | C(2,6)H 7.04; C(3,5)H 6.79 |
| $Ile^{28}$ | 8.36 | 3.74 | 1.89 | 1.65, 1.14 | $C^{\gamma}H_3$ 0.86; $C^{\delta}H_3$ 0.81 |
| $Asn^{29}$ | 8.17 | 4.44 | 2.85, 2.77 | | $N^{\delta}H_2$ 7.45, 6.83 |
| $Leu^{30}$ | 7.76 | 4.07 | 1.60, 1.40 | 1.45 | $C^{\delta}H_3$ 0.75; $C^{\delta}H_3$ 0.68 |
| $Ile^{31}$ | 7.95 | 3.97 | 1.87 | 1.48, 1.12 | $C^{\gamma}H_3$ 0.81; $C^{\delta}H_3$ 0.68 |
| $Thr^{32}$ | 7.94 | 4.18 | 4.29 | 1.22 | |
| $Arg^{33}$ | 7.82 | 4.24 | 1.90, 1.86 | 1.68 | $C^{\delta}H_2$ 3.16; $N^{\epsilon}H$ 7.14; $N^{\eta}H_2$ 6.64 |
| $Gln^{34}$ | 8.01 | 4.24 | 2.05, 2.00 | 2.34 | $N^{\epsilon}H_2$ 6.78, 7.40 |
| $Arg^{35}$ | 8.12 | 4.21 | 1.67 | 1.47, 1.40 | $C^{\delta}H_2$ 3.10; $N^{\epsilon}H$ 7.13; $N^{\eta}H_2$ 6.64 |
| $Tyr^{36}$ | 8.00 | 4.57 | 3.11, 2.89[b] | | C(2,6)H 7.14; C(3,5)H 6.80 |
| $NH_2$ | | | | | 7.04, 7.41 |

[a] In 90% $H_2O$/10% $D_2O$ at 37 °C and pH 3.2. Chemical shifts are for the major conformer and are given in ppm, referenced to DSS at 0 ppm. For methylene protons, two chemical shifts are given only when both resonances could be resolved.
[b] Stereospecifically assigned resonances. For the $C^{\beta}H$ resonances, the first chemical shift is for $H^{\beta 2}$ (pro-*R*), and the second for $H^{\beta 3}$ (pro-*S*) (IUPAC-IUB, 1970).

*NMR resonance assignment*

Proton resonance assignments for human NPY were made using the standard sequential assignment procedure (Wüthrich, 1986), in which extensive use was made of TOCSY spectra in $H_2O$ to define complete amino acid spin systems commencing at the backbone amide proton (Chazin and Wright, 1987). As these methods are well established, details of the assignment procedure will not be documented here; the range of 2D experiments used is summarised in the Methods.

Our assignments for human NPY are similar to those of Saudek and Pelton (1990) for porcine NPY (which has leucine at position 17 instead of methionine), the major difference being that the NH resonances of $Asp^{6}$ and $Asn^{7}$ are inverted. There are also a few minor differences in the chemical shifts of the N-terminal residues (Table 1), and the $Gly^{9}$ $C^{\alpha}H_2$ and the $Leu^{24}$ $C^{\delta}H_3$ resonances are degenerate under our conditions, while the $Asp^{11}$ $C^{\beta}H_2$, $Arg^{19}$ $C^{\gamma}H_2$, $Arg^{35}$ $C^{\gamma}H_2$ and the C-terminal amide resonances are not, in contrast to the published assignments for porcine NPY. The fingerprint $C^{\alpha}H$-NH and backbone NH-NH regions of a 200 ms NOESY spectrum of human NPY recorded in $H_2O$ at pH 3.2 and 37 °C are shown in Fig. 2.

Figure 3 summarises the type of sequential NOE connectivities (i,i + 1) on which the specific assignments are based, together with estimates of the three-bond NH to $C^{\alpha}H$ coupling constants and the location of the medium-range NOE connectivities. The presence of $d_{\alpha N}$ (i,i + 3), $d_{\alpha\beta}$ (i,i+3) and $d_{\alpha N}$ (i,i+4) NOEs spanning residues 13–36 is indicative of an α-helical structure in this region

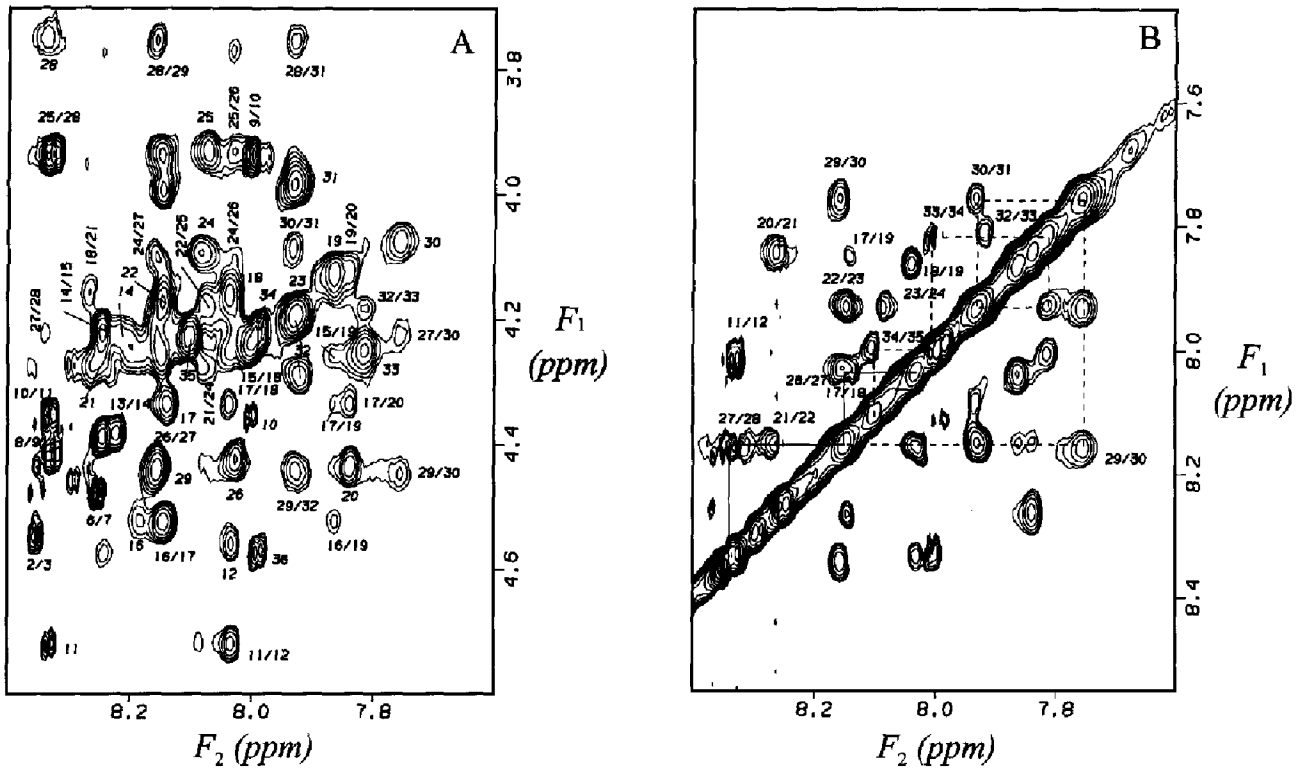


Fig. 2. Regions of a 200 ms NOESY spectrum of human NPY in $H_2O$ at pH 3.2 and 37 °C recorded at 600 MHz. (A) Fingerprint region showing intraresidue NH-C$^{\alpha}$H, sequential (i,i + 1), and medium-range C$^{\alpha}$H-NH (i,i + 2; i,i + 3; i,i + 4) cross peaks from the α-helix. Resonances from Asp$^{6}$ are not shown. (B) Backbone amide region showing sequential NH-NH connectivities between residues 11–34. The $d_{NN}$ (28,29) cross peak is overlapped with that for $d_{NN}$ (27,28).

(Wüthrich, 1986). Chemical shift index analysis (Wishart et al., 1992; Wishart and Sykes, 1994) of the C$^{\alpha}$H and C$^{\alpha}$ resonances also supports the existence of a helix in this region of the molecule (Fig. 4). At 30 °C, exchange of the backbone amides in $D_2O$ was too fast to be measured by 1D spectra, while at lower temperatures resonance broadening and peak overlap prevented the unequivocal identification of slowly exchanging amides.

As in the 2D spectra of porcine NPY (Saudek and Pelton, 1990), our spectra of human NPY revealed the existence of multiple conformations, with one or more resonances from residues 1–10, as well as those of Tyr$^{20}$, being affected. Splitting of peaks from the N-terminal residues may be attributed to cis–trans isomerism of one or more of the proline residues at positions 2, 5 and 8. Both major forms of Pro$^{8}$ showed $d_{\alpha\delta}$ NOESY connectiv-

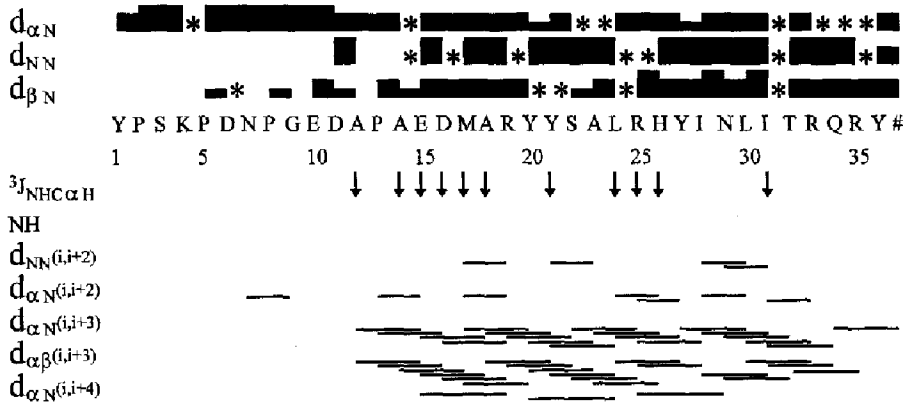


Fig. 3. Summary of the NMR data used in the sequential assignment and secondary structure determination of human NPY. Filled bars indicate sequential connectivities observed in a 200 ms mixing time NOESY spectrum of the polypeptide in $H_2O$ at pH 3.2 and 37 °C. The height of the bar indicates the strength of the NOE, categorised as strong, medium or weak. Shaded bars represent $d_{\alpha\delta}$ (i,i + 1) connectivities to proline residues. Connectivities that could not be identified because of peak degeneracy or overlap with the residual water resonance are indicated with asterisks (*). Arrows indicate $^{3}J_{NHC^{\alpha}H}$ coupling constants of < 6.0 Hz. Medium-range NOE connectivities are also shown, but in this case the height of the bar does not indicate the strength of the NOE. # denotes the amidated C-terminus.

ities, consistent with a trans conformation. In $Pro^2$, the $C^{\alpha}H$ chemical shift was so close to that of $Tyr^1$ that a possible $d_{\alpha\alpha}$ connectivity in the minor form could not be resolved from the diagonal; the major form clearly showed a $d_{\alpha\delta}$ connectivity. For $Pro^5$, neither $d_{\alpha\alpha}$ nor $d_{\alpha\delta}$ NOESY connectivities were observed because of overlap of the $Lys^4$ $C^{\alpha}H$ resonance with the residual water signal. These observations differ from those for human NPY reported by Darbon et al. (1992), in which the resonances of all residues except $Lys^4$ and $Asn^7$ reflected a single conformation. Our 1D spectra of human NPY also showed a marked concentration dependence, with sharper and better resolved signals observed at concentrations below 2 mM, whereas Darbon et al. (1992) stated that the line widths were independent of concentration over the range 4.0 to 0.04 mM. The aromatic regions of spectra of human NPY at concentrations of 4 and 1 mM in $D_2O$ at 37 °C are shown in Fig. 5. At the lower concentration (Fig. 5B), the signals for the imidazolium ring protons of $His^{26}$ and the aromatic protons of $Tyr^{20}$ and $Tyr^{27}$ were clearly split into two (ratio 2:1); at the higher concentration, peak broadening made it difficult to establish if both sets of peaks were still present or to measure their ratios (Fig. 5A). The peak splitting pattern seen for human NPY was also observed in the 1D spectrum of porcine NPY (Fig. 5C). Coalescence of the split signals in this spectrum was achieved at 75 °C and the process was reversible on cooling to 37 °C. At 75 °C, peak splitting from the N-terminal residues, which is assumed to arise

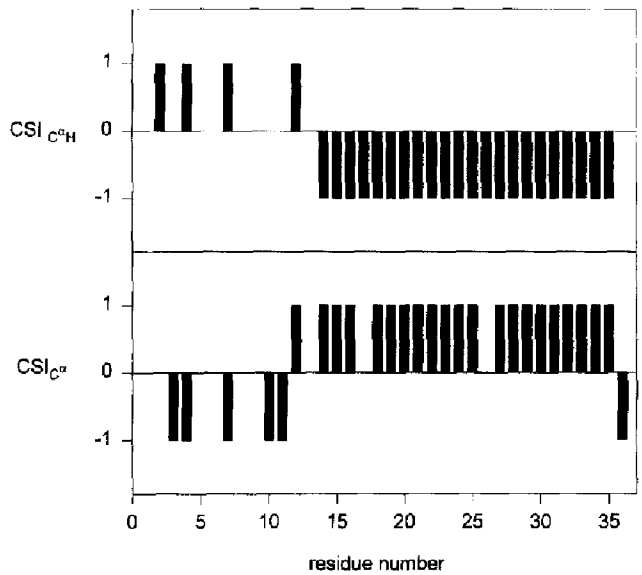


Fig. 4. Chemical shift index (CSI) analyses (Wishart et al., 1992; Wishart and Sykes, 1994) for human NPY at pH 3.2 and 37 °C. (A) The CSI is given as +1 if the $C^{\alpha}H$ resonance is >0.1 ppm downfield from its random coil value, −1 if >0.1 ppm upfield, or 0 if it is close to its random coil value (Wishart et al., 1995). (B) The CSI is given as +1 if the $C^{\alpha}$ resonance is >0.7 ppm (4.0 ppm for proline) downfield from its random coil value, −1 if >0.7 ppm (4.0 ppm for proline) upfield, or 0 if it is close to its random coil value (Wishart et al., 1995).

from cis–trans isomerisation of one or more of the prolines, was still evident. HPLC profiles of the samples after 1D NMR analysis showed a single peak, indicating that the splitting was not due to sample degradation, and the same splitting was observed with a separate sample of synthetic porcine NPY obtained from Drs. R. Murphy and J. Angus (University of Melbourne, Parkville, Australia). At this stage, the origin of this peak splitting is unclear.

*Structure of the monomer*

Structures were generated using a set of 494 distance restraints inferred from NOEs, and 11 backbone and 4 side-chain dihedral angle restraints derived from spin–spin coupling constants. The distance restraint set, from which values redundant with the covalent geometry had been eliminated, consisted of 149 intraresidue, 91 sequential and 200 medium-range ($i-j \leq 4$) upper bounds, as well as 54 lower bounds. A total of 24 long-range NOEs ($i-j \geq 4$) were excluded from the calculations, as these distances were not compatible with structures calculated using the 494 distance restraints and thus could not be attributed to intramolecular contacts. Attempts at structure calculations using the full set of NOE constraints failed, presumably as a result of strongly violated distance constraints (DIANA would not run when the 24 long-distance NOEs were included). Structures were calculated using DIANA, and were then refined by simulated annealing in X-PLOR and energy minimised using the CHARMm force field.

The rms differences for the backbone heavy atoms when the final 26 structures were superimposed over the entire sequence are shown as a function of residue number in Fig. 6A. These data indicate that the structure is better defined in the C-terminal than in the N-terminal region, while the backbone angular order parameters (Figs. 6B and C) are well defined ($S > 0.8$) for residues 11–36. When the structures were superimposed over residues 11–36, mean pairwise rms differences of 0.51 and 1.34 Å were obtained for the backbone heavy atoms (N, $C^{\alpha}$, C) and all heavy atoms, respectively. Corresponding values for the entire molecule were much larger, at 4.73 and 5.24 Å, respectively, reflecting the poor definition in the N-terminus. Based on the $\phi$ and $\psi$ angles of the angular average of the 26 structures and on the hydrogen bonding pattern (see below), a helix extends from residues 13 to 36, for which the rms differences were 0.42 and 1.30 Å, respectively. Stereoviews of the 26 final structures, superimposed over the backbone heavy atoms of residues 11–36, are shown in Fig. 7.

In the C-terminal helix, $NH_{i+4} \rightarrow CO_i$ hydrogen bonds were observed from residues 36 to 12 in most of the structures, except for the $20 \rightarrow 16$ bond, which was present in only half the structures, and the $25 \rightarrow 21$ and $33 \rightarrow 29$ bonds, which were not present in any structure. In-

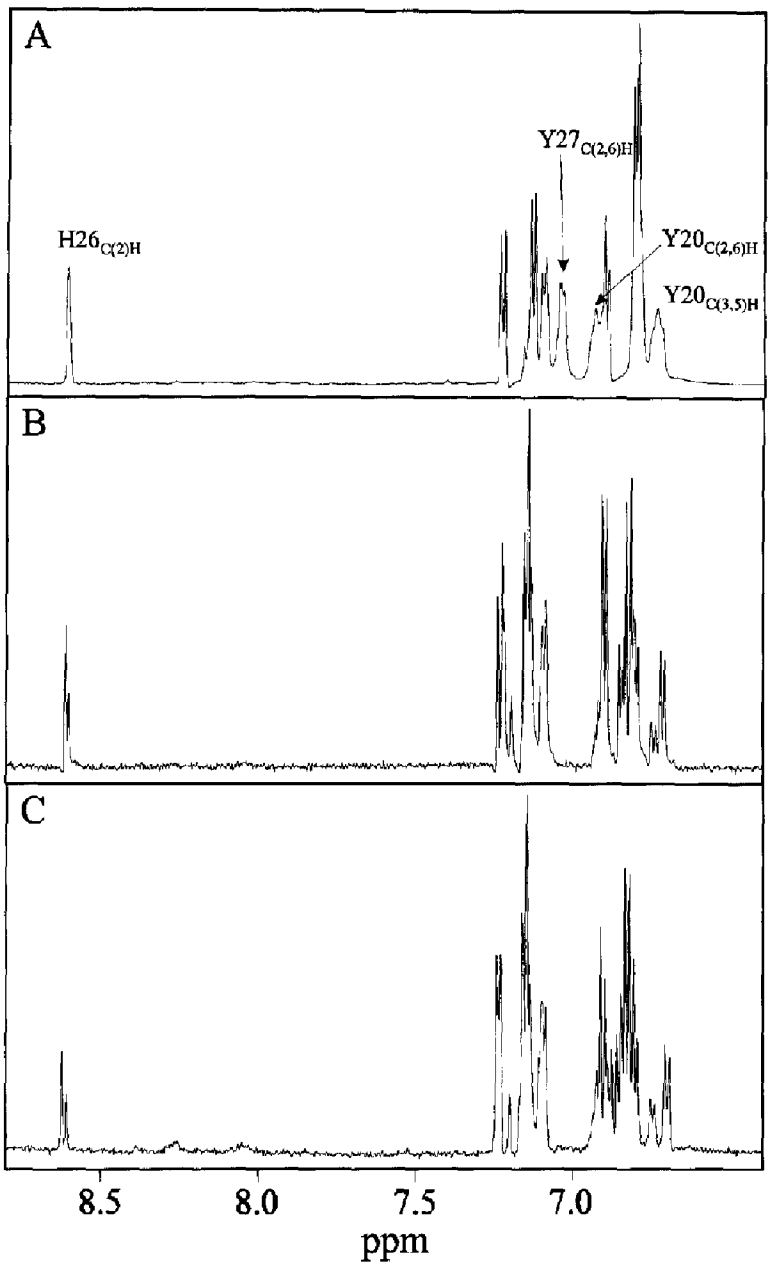


Fig. 5. Aromatic regions of 1D spectra of NPY in $D_2O$, recorded at 600 MHz and 37 °C for (A) 4 mM human NPY, pH 3.2; (B) 1 mM human NPY, pH 3.3; and (C) 1 mM porcine NPY, pH 3.1.

spection of the $\phi$ and $\psi$ angles of the angular average of the 26 structures indicates that the helix is kinked around the 21–22 peptide bond, and this kink is reflected in the presence of $21 \rightarrow 18$ and $25 \rightarrow 20$ hydrogen bonds in all the structures. Two $NH_{i+3} \rightarrow CO_i$ hydrogen bonds, $30 \rightarrow 27$ and $15 \rightarrow 12$, were also observed in the helical region. In the N-terminal region, a $9 \rightarrow 7$ bond was observed and the $\phi$ and $\psi$ angles for residue 8, which are well defined (Fig. 6), are consistent with the presence of an inverse $\gamma$-turn at this position. Several hydrogen bonds involving side chains in the helix were also apparent, and one of the C-terminal amide protons formed hydrogen bonds to the backbone carbonyl of $Gln^{34}$.

*Structure of the dimer*

Using the protocol of Nilges (1993) for the structure calculation of symmetric dimers from NMR data, the 24 distance constraints classified as intersubunit (Fig. 8) proved to be consistent with a dimer structure, as no significant distance constraint violations were observed. Except for the initial 12 residues and the last 2, the final dimer structure was well defined, with a mean pairwise rmsd for the backbone heavy atoms (N, $C^{\alpha}$, C) of 0.90 Å. The NPY dimer comprises antiparallel packing of the monomeric helical units, with the hydrophobic interactions arising mainly between tyrosine and isoleucine side chains forming the dimer interface. Figure 9 shows a

stereoview of the NPY dimer structure which was closest to the average.

## Discussion and Conclusions

Human NPY self-associates in aqueous solution at the concentration (4–5 mM) used in this NMR study. Sedimentation equilibrium experiments performed under conditions similar to those of the NMR experiments indicated that dimers were the main species present in solution and that higher aggregates, most likely tetramers, were also present, at least in the presence of salt. In the absence of added salt, the nature of the NPY molecules at either low or high concentrations could not be determined by sedimentation analysis because of nonideal behaviour associated with the highly charged state of the peptide at pH 3. To confirm that the observed intermolecular NOEs were due primarily to helix–helix interactions in a dimer, NOESY spectra were acquired at 1 mM in the absence and presence of NaCl, where the fraction of higher order aggregates would have been reduced, and were found to contain most of the intermolecular NOEs detected at the higher NMR sample concentration. Those intermolecular NOEs which were still clearly observable at the lower concentration were consistent with the dimer structure shown in Fig. 9. Another possible explanation for these NOEs is that they represent long-range interactions in a monomer that is not constrained in a helical conformation. From published circular dichroism spectra, it appears that at low concentrations (< 0.1 mM) and acidic pH values, the helical content of NPY is indeed lower than at higher concentrations and/or neutral pH (Minakata et al., 1989; Saudek and Pelton, 1990; Mierke et al., 1992), although some amount of helix is still present (Minakata et al., 1989). However, these spectra also imply that in the absence of helix the structure is largely unordered, and unordered polypeptides in aqueous solution at ambient temperatures typically show few medium-range and no long-range NOEs because of conformational averaging and decreased effective correlation times. We believe, therefore, that the long-range NOEs are intermolecular in origin, and that the dimer structure described here represents a significant fraction of human NPY under our solution conditions. It must be borne in mind, however, that the dimer is in equilibrium with monomer and higher aggregates (possibly tetramers), and

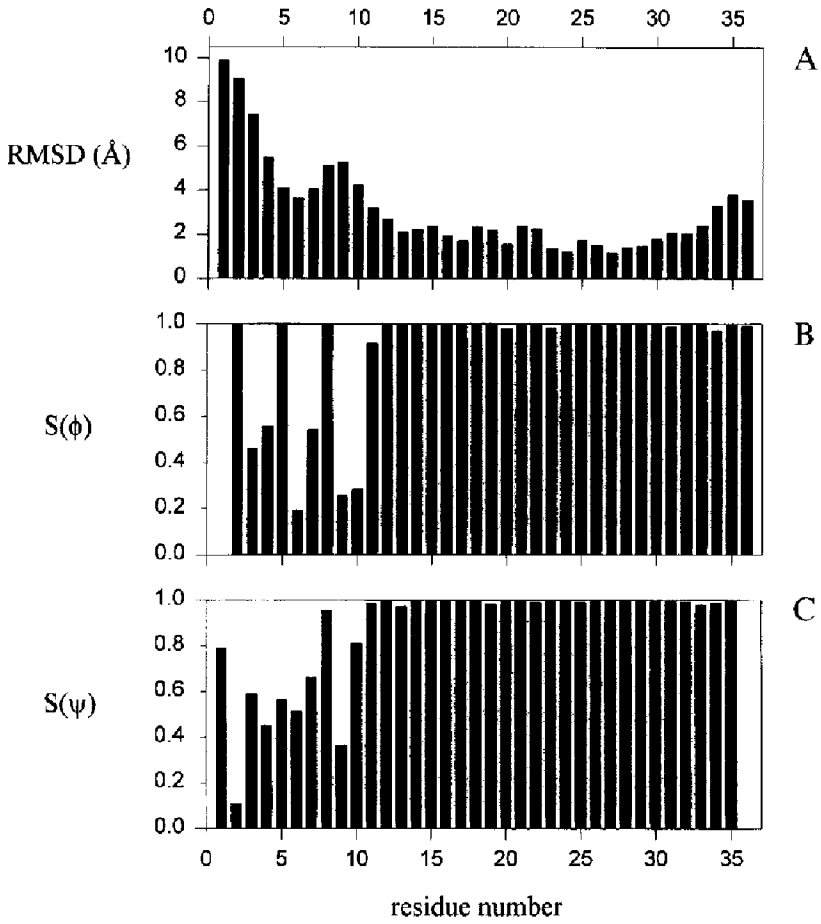


Fig. 6. Parameters characterising the final family of structures for human NPY monomer, plotted as a function of residue number. (A) Rmsd from the mean structure for the backbone heavy atoms (N, $C^{\alpha}$ and C) when the 26 final structures are superimposed over the entire length of the molecule. (B and C) Angular order parameters (Hyberts et al., 1992; Pallaghy et al., 1993) for the backbone dihedral angles $\phi$ and $\psi$, respectively.

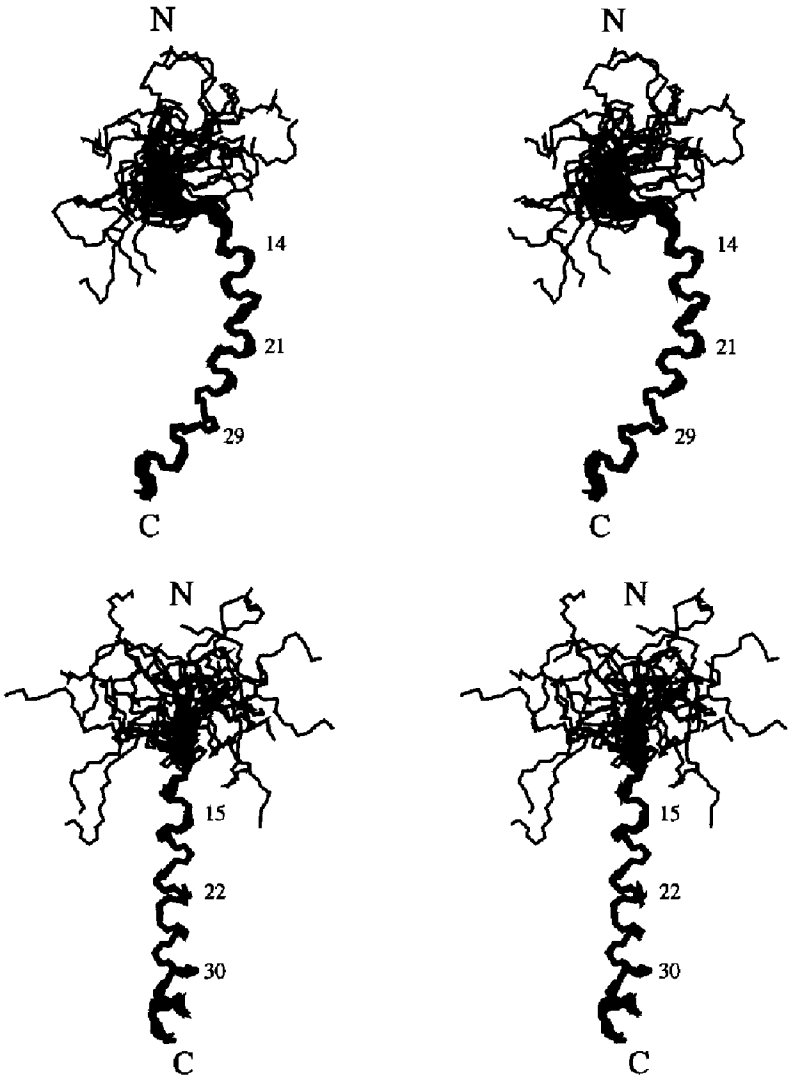


Fig. 7. Stereoviews of the 26 final structures of human NPY monomer, superimposed over the backbone heavy atoms (N, $C^{\alpha}$ and C) of residues 11–36. The two views are related by a rotation of approximately 90° around the vertical axis.

in both of these forms the local conformation may vary from the average observed spectroscopically.

Analysis of the line widths in the aromatic region of the 1D spectrum showed that the terminal tyrosine residues ($Tyr^{1}$ and $Tyr^{36}$) displayed greater conformational freedom than the three inner ones ($Tyr^{20}$, $Tyr^{21}$ and $Tyr^{27}$), which is consistent with the notion that the inner tyrosine residues are involved in helix–helix packing interactions that make this part of the molecule less mobile than the N- and C-termini. Similar observations were reported for porcine NPY (Cowley et al., 1992).

The main secondary structure element in human NPY is an amphipathic α-helix spanning residues 13–36. This observation is consistent with the structure of porcine NPY, where the helix extended all the way to the C-terminus (Cowley et al., 1992). By contrast, the structure of human NPY in aqueous solution determined by Darbon et al. (1992) differs significantly from both our structure and that of porcine NPY. The structure proposed by Darbon et al. (1992) is in general agreement with the PP-fold structure of avian PP (Blundell et al., 1981) and bovine PP (Li et al., 1992), but these authors found no evidence of dimer formation. They concluded that human NPY consists of two short contiguous α-helices made up of residues 15–26 and 28–35, with the first helix (15–26) connected to the polyproline region (residues 1–10) by a tight hairpin turn (residues 11–14). However, a hairpin fold in that region of the molecule is not compatible with the measured coupling constants and pattern of NOEs in our NMR spectra. The presence of a kink at position 27 in the human NPY structure of Darbon et al. (1992) is also not compatible with the pattern of medium- and long-range NOEs detected in our spectra. In our structure of human NPY there is a kink around residues 21–22.

One reason for the differences between the human NPY structure of Darbon et al. (1992) and ours is the difference in the number and type of NOEs detected and hence the distance constraints used in the structure calcu-

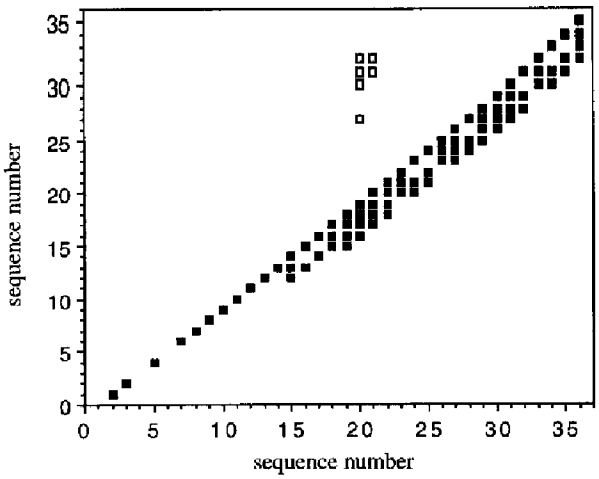


Fig. 8. Distribution of NOEs over the sequence of human NPY within the monomer (■) and between monomers (□).

lations. The structure of Darbon et al. (1992) was based on a set of 263 distance restraints, consisting of 101 intraresidual, 48 sequential, 60 medium range and 54 long range. In our study, a final set of 440 upper bound distance restraints was used, consisting of 149 intraresidual, 91 sequential, 200 medium range and 24 long range (interpreted as intermolecular NOEs). The large number and distribution of medium-range NOEs detected in our study gave rise to the well-defined α-helix in our structures. In fact, it is possible to observe clear differences between cross peaks in the fingerprint region of the 200 ms NOESY spectrum published by Darbon et al. (1992) and those in our study. For example, the sequential NOEs between residues 11/12, 16/17, 17/18, 19/20, 26/27, 27/28 and 29/30, as well as the $d_{\alpha N}$ (i,i+3) NOEs between 16/19, 17/20, 24/27 and 29/32 were not evident in their fingerprint region but were clearly detected in our spectra. Several of these NOE cross peaks missing from the spectrum of Darbon et al. (1992) occur near the residual water signal at 4.65 ppm. There are also a few differences in the NOEs detected in the amide region; in the spectrum of Darbon et al. (1992) a $d_{NN}$ (15,16) connectivity was detected which was not observed in our spectra, but if it were, it would have occurred at a more downfield position than the cross peak assigned by Darbon et al. (1992). Also, there is a significant difference in the position of the $d_{NN}$ (17,18) cross peak; in our spectrum this cross peak is partially overlapped with the $d_{NN}$ (26,27) cross peak (but is clearly resolved in a spectrum run at a slightly higher pH), whereas in the spectra of Darbon et al. (1992) the signal assigned to $d_{NN}$ (17,18) is more downfield and is not detected in our spectra. The cross peak assigned to $d_{NN}$ (17,18) in our NOESY spectrum is present in a similar position in the spectrum of Darbon et al. (1992), but has not been assigned there. Despite the fact that there is no chemical shift assignment table given for the human NPY structure determined by Darbon et al. (1992), we have found differences in the relative position of several NOEs detected in their NOESY spectrum as compared to our data, which may be attributable to minor differences in the solution conditions used. Our chemical shift assignments are similar to the published assignments for porcine NPY (Saudek and Pelton, 1990), except for the NH resonances of residues 6 and 7 and minor differences in the NH and $C^{\alpha}H$ shifts of the charged residues in the N-terminus. Some of these differences may be due to the presence of 0.05 M deuterated acetic acid in the sample of Saudek and Pelton (1990).

It is also clear from our 1D spectra, recorded at several different concentrations of human NPY, that the spectra were concentration dependent, becoming significantly sharper at low concentration, and that at lower concentrations additional peak splittings appeared. This was not reported in the paper of Darbon et al. (1992), even though they recorded spectra over an even greater concentration range. At this stage we are unable to explain this disagreement.

Our model for the dimer of human NPY is consistent with that proposed for porcine NPY by Cowley et al. (1992), in that the two NPY molecules interact via their helices and are in an antiparallel arrangement. In fact, the

Fig. 9. Stereoview of the NPY dimer structure closest to the average calculated structure. Note that only the helical residues are well defined in these structures; the orientation of the N-termini relative to the helices varies greatly.

number of intermolecular NOEs is the same (24) in both structures. Compared with the porcine structures, however, the helices in our structures are not as closely intertwined in the dimer (Fig. 9). Furthermore, there is greater variation in the orientation of the N-termini relative to the helices in our structures (Fig. 7). To some extent, these differences are reflections of the limited number of intermolecular NOEs used as restraints, which dictates that the relative orientation of the two subunits in the dimer is not as well defined as the structures of the subunits themselves. The involvement of tyrosine residues in the hydrophobic interface of the porcine NPY dimer, inferred from fluorescence studies (Cowley et al., 1992), is also consistent with our NMR data for the human dimer, where intermolecular NOEs from the aromatic protons of $Tyr^{20}$ to side-chain protons of $Leu^{30}$ and $Ile^{31}$ and to the aromatic protons of $Tyr^{27}$ were observed.

Dimerisation in solution has been described previously for mammalian PPs (Chang et al., 1980; Noelken et al., 1980) and for NPYs (Minakata et al., 1989), and in the crystalline state avian PP exists as a dimer. Thus, it seems likely that this family of peptides forms dimers (and possibly higher aggregates) at moderate concentrations in solution. The biological significance of dimer formation is difficult to assess, but self-associated forms of NPY may well be present in its storage form and it is noteworthy that in both human and porcine NPY dimer formation brings the N- and C-termini of the two monomeric units into much closer proximity than in the isolated monomers. Juxtaposition of the termini appears to be a requirement for receptor binding, particularly to the $Y_1$ receptor (Grundemar et al., 1993; Grundemar and Håkanson, 1994).

## Acknowledgements

This work was supported in part by the Australian Cooperative Research Centre for Biopharmaceutical Research Pty. Ltd. We thank Dr. Mark Duncan, Biomedical Mass Spectrometry Unit, University of New South Wales, for providing the mass spectral analysis, Lisa Cowen and John McFarlane for assistance with computing, and one of the referees for helpful comments.

## References

Anil Kumar, Ernst, R.R. and Wüthrich, K. (1980) *Biochem. Biophys. Res. Commun.*, **95**, 1–6.

Barden, J.A. (1995) *Biochem. Biophys. Res. Commun.*, **215**, 264–271.

Bax, A., Griffey, R.H. and Hawkins, B.L. (1983) *J. Am. Chem. Soc.*, **105**, 7188–7190.

Blundell, T.L., Pitts, J.E., Tickle, I.J., Wood, S.P. and Wu, C.-W. (1981) *Proc. Natl. Acad. Sci. USA*, **78**, 4175–4179.

Boulanger, Y., Chen, Y., Commodari, F., Senécal, L., Laberge, A.-M., Fournier, A. and St. Pierre, S. (1995) *Int. J. Pept. Protein Res.*, **45**, 86–95.

Braunschweiler, L. and Ernst, R.R. (1983) *J. Magn. Reson.*, **53**, 521–528.

Brooks, B.R., Bruccoleri, R.E., Olafson, B.D., States, D.J., Swaminathan, S. and Karplus, M. (1983) *J. Comput. Chem.*, **4**, 187–217.

Brünger, A.T. (1992) *X-PLOR v. 3.1, A System for X-ray Crystallography and NMR*, Yale University, New Haven, CT, U.S.A.

Chang, P.J., Noelken, M.E. and Kimmel, J.R. (1980) *Biochemistry*, **19**, 1844–1849.

Chazin, W.J. and Wright, P.E. (1987) *Biopolymers*, **26**, 973–977.

Colmers, W.F. and Wahlestedt, C. (1993) *The Biology of Neuropeptide Y and Related Peptides*, Humana, Totowa, NJ, U.S.A.

Cowley, D.J., Hoflack, J.M., Pelton, J.T. and Saudek, V. (1992) *Eur. J. Biochem.*, **205**, 1099 1106.

Darbon, H., Bernassau, J.-M., Deleuze, C., Chenu, J., Roussel, A. and Cambillau, C. (1992) *Eur. J. Biochem.*, **209**, 765 771.

Fogolari, F., Esposito, G., Cauci, S. and Viglino, P. (1993) *J. Magn. Reson.*, **A102**, 49–57.

Gray, T.S. and Morley, J.E. (1986) *Life Sci.*, **38**, 389–401.

Griesinger, C., Sørensen, O.W. and Ernst, R.R. (1987) *J. Magn. Reson.*, **75**, 474–492.

Grundemar, L., Sheikh, S.P. and Wahlestedt, C. (1993) In *The Biology of Neuropeptide Y and Related Peptides* (Eds., Colmers, W.F. and Wahlestedt, C.), Humana, Totowa, NJ, U.S.A., pp. 197–239.

Grundemar, L. and Håkanson, R. (1994) *Trends Pharmacol. Sci.*, **15**, 153–158.

Güntert, P., Braun, W. and Wüthrich, K. (1991) *J. Mol. Biol.*, **217**, 517–530.

Hyberts, S.G., Märki, W. and Wagner, G. (1987) *Eur. J. Biochem.*, **164**, 625–635.

Hyberts, S.G., Goldberg, M.S., Havel, T.F. and Wagner, G. (1992) *Protein Sci.*, **1**, 736–751.

IUPAC-IUB Commission on Biochemical Nomenclature (1970) *J. Mol. Biol.*, **52**, 1–17.

Li, X., Sutcliffe, M.J., Schwartz, T.W. and Dobson, C.M. (1992) *Biochemistry*, **31**, 1245–1253.

Macura, S., Huang, Y., Suter, D. and Ernst, R.R. (1981) *J. Magn. Reson.*, **43**, 259–281.

Marion, D. and Wüthrich, K. (1983) *Biochem. Biophys. Res. Commun.*, **113**, 967–974.

Mierke, D.F., Dürr, H., Kessler, H. and Jung, G. (1992) *Eur. J. Biochem.*, **206**, 39–48.

Minakata, H., Taylor, J.W., Walker, M.W., Miller, R.J. and Kaiser, E.T. (1989) *J. Biol. Chem.*, **264**, 7907–7913.

Nilges, M. (1993) *Proteins*, **17**, 297 309.

Noelken, M.E., Chang, P.J. and Kimmel, J.R. (1980) *Biochemistry*, **19**, 1838–1843.

Pallaghy, P.K., Duggan, B.M., Pennington, M.W. and Norton, R.S. (1993) *J. Mol. Biol.*, **234**, 405–420.

Pallaghy, P.K., Scanlon, M.J., Monks, S.A. and Norton, R.S. (1995) *Biochemistry*, **34**, 3782–3794.

Rucker, S.P. and Shaka, A.J. (1989) *Mol. Phys.*, **68**, 509–517.

Saudek, V. and Pelton, J.T. (1990) *Biochemistry*, **29**, 4509–4515.

Schachman, H.K. (1959) *Ultracentrifugation in Biochemistry*, Academic Press, New York, NY, U.S.A., pp. 201–247.

Wagner, G., Braun, W., Havel, T.F., Schaumann, T., Gō, N. and Wüthrich, K. (1987) *J. Mol. Biol.*, **196**, 611–639.

Wishart, D.S., Sykes, B.D. and Richards, F.M. (1992) *Biochemistry*, **31**, 1647–1651.

Wishart, D.S. and Sykes, B.D. (1994) *J. Biomol. NMR*, **4**, 171 180.

Wishart, D.S., Bigam, C.G., Holm, A., Hodges, R.S. and Sykes, B.D. (1995) *J. Biomol. NMR*, **5**, 67–81.

Wüthrich, K. (1986) *NMR of Proteins and Nucleic Acids*, Wiley, New York, NY, U.S.A.